JJMIE

Volume 16, Number 5, December. 2022
ISSN 1995-6665
Pages 677– 688

Jordan Journal of Mechanical and Industrial Engineering

Performance Enhancement of Multi-Modal Piezoelectric Energy Harvesting Through Parameter Optimization

Ossama Mokhiamar[1, *], David Omooria Masara[1,2], Hassan El Gamal[1]

[1] Alexandria University, Faculty of Engineering, Mechanical Engineering Department, El-Chatby, Alexandria 21544, Egypt

[2] University of Eldoret, School of Engineering, Department of Mechanical and Production Engineering, 1125-30100, Eldoret, Kenya

Received 19 Apr 2022 Accepted 13 Sep 2022

Abstract

This study presents an optimized multi-resonant piezoelectric energy harvester to scavenge broadband energy over a frequency range between 11 Hz -17 Hz. The harvester encompasses a rectangular beam with two parallel splits to form three branches. The branches are of unequal length and width. End masses of dissimilar sizes were affixed at the ends of each branch to tailor the resonant frequencies. A piezoelectric material was laid on both sides of the driving beam to form a bimorph. The initial parameters of the harvester were obtained from a parametric study using the Finite Element Method. COMSOL Multiphysics software was used to apply boundary conditions to the design and to perform the optimization. The Bound Optimization by Quadratic Approximation (BOBYQA) algorithm was deployed in optimization because of its versatility in derivative-free, bound-constrained optimization problems. In comparison to its unoptimized form, a 31.67% average power increment was realized from the design. The optimal impedance was reduced from 5.62 kΩ to 1.778 kΩ, which enhances the efficiency of the harvester by reducing electrical damping. The proposed optimized harvester was compared to a Multi-Resonant Piezoelectric Energy Harvester for verification. It was shown to be more effective by harvesting sufficiently higher broadband energy.

Keywords: piezoelectric energy harvesting; optimization; low-frequency; multimodal.

Nomenclature

c	Damping coefficient matrix
c_p	Capacitance of the piezoelectric material
k	Stiffness matrix
m	Mass matrix of the harvester
m_1	Mass on Branch 1
m_2	Mass on Branch 2
m_3	Mass on Branch 3
R	Load resistance
v	Induced voltage
x	Harvester displacement
y	Base displacement
w_1	Width of Branch 1
w_2	Width of Branch 2
w_3	Width of Branch 3
d_{31}, d_{33}, d_{15}	Piezoelectric Constants
T_1, T_2 and T_3	Normal Stresses in x, y, and z Axes
T_4, T_5 and T_6	Shear Stresses
E (superscript)	Zero or Constant Electric Field
T (superscript)	Zero or Constant Stress Field
t (superscript)	Transpose of a Matrix
$\ddot{x}, \ddot{y}, \ddot{z}$	Harvester acceleration, Base acceleration, Relative acceleration
$\dot{z}$, z	Relative velocity and displacement vector tensors respectively.
$\{D\}$	Electrical Displacement Tensor
$\{E\}$	Electric Field Tensor
$\{T\}$	Mechanical Stress Tensor
$\{s\}$	Mechanical Strain Tensor
$[d]$	Direct Piezoelectric Matrix
$[s^E]$	Electric compliance matrix
α	Effective electromechanical coupling coefficient
ω	Vibration frequency in rad/s
$[\varepsilon]$	Permittivity Matrix

Abbreviations

CPEH	Conventional Piezoelectric Energy Harvester
DOF	Degrees of Freedom
FEM	Finite Element Method
MRPEH	Multi-Resonant Piezoelectric Energy Harvester

* Corresponding author e-mail: usamam@alexu.edu.eg.

PEH	Piezoelectric Energy Harvester
PZT	Lead zirconate Titanate
SCMEH	Split Cantilever Multi-Resonant Energy Harvester

1. Introduction

The advancement in technology, especially in automation, structural health monitoring(SHM), predictive maintenance [1] and the Internet of Things (IoT), has triggered the need for self-powered microelectronic devices. Previously, such devices primarily drew their power from depletable chemical batteries that required periodic replenishment. Such batteries are hazardous to the environment at the end of their useful life, as noted by Lange et al [2] , that the sharp rise in energy usage has posed serious environmental consequences. The mechanical-to-electrical transduction mechanisms used include electromagnetic transduction, electrostatic transduction, and mainly piezoelectric transduction. Piezoelectric transduction involves the use of piezoelectric materials laid on one or both sides of a mechanical beam. When the composite is subjected to vibrations, the elastic substrate beam deforms and strains the piezoelectric material. Piezoelectricity is thus induced under strain to generate electrical energy. The harvesters possess different configurations spanning from narrow bandwidth harvesters that operate on a sole resonant frequency to multimodal harvesters with more than one operational resonant frequency. The essence of energy harvesting is to complement replaceable batteries and provide a sustained energy supply for microelectronic devices. Energy harvesters, therefore, offer a theoretically perpetual power source to enhance autonomy and prognostics. As a result, vibration, an otherwise unsolicited phenomenon, can be put to valuable use like charging mobile devices [3].

A harvester must discharge vital power to a specified electrical load (appliance) for extended periods to be efficient. For this motive, the energy from a harvester should be maximized with diminutive alteration to the existing constraints such as space and vibration source frequencies. One primary method of accomplishing power maximization is through optimization. Optimization is a technique that has been widely deployed in many forms, such as: stochastic and deterministic optimization, shape optimization, geometry optimization, and topology optimization. Hybridization is a technique whereby more than a single transduction method is deployed in attempts to optimize harvesters, although Ahmad et al. highlighted the benefits of using a standalone device [4]. Besides these techniques, optimization has been capacitated through increasing the electromechanical coupling. For instance, Cho et al. [5] highlighted the impact of piezoelectric residual stress and coverage of the electrodeon the electrical coupling coefficient. It was concluded that the optimum coupling was achieved at an electrode coverage of 60%. Wang and Wu further investigated the impact of piezoelectric patch positioning and measurements on the performance of a cantilever harvester. It was inferred that the efficiency decreases as the position of the piezoelectric patch moves away from the fixed end of the beam. In an attempt to maximize the power output, beams with initial curvature were also exploited by Yoon et al. [7]. Elahi [8], on the other hand, inferred that the piezoelectric material and substrate length ratio had a significant impact on the performance of the harvester. Elahi et al. [9] proved that a rectangular patch is more efficient than a circular patch, and the length of the patch in relation to the driving beam length affects the harvester's performance. For instance, equal lengths of aluminum substrate combined with a PZT-5A piezoelectric material were reported to have the maximum voltage induced at the utmost tip displacement.

Topology optimization entails material removal and/or material orientation such that the material is deposited at a location where its maximum performance can be achieved. Acciani et al. [10] realized a 16% increase in harvested energy efficiency from a multimodal device. The increment was achieved by varied material removal from the said structure. A differential configuration is used to achieve maximum efficiency. Kim and Shin [11] reported a topologically optimized harvester. A method to optimize material layout was developed using a semi-empirical equation for electromechanical coupling. Various piezoelectric materials were tested, and enhanced efficiency was realized for all of them. Lee and Tovar [12] optimized an energy harvesting skin using a Hybrid Cellular Automata. The domain is discretized to form Cellular Automata, and the output power is maximized by finding optimum densities and polarizing directions in every Automata. Later, Thein and Liu [13] performed a two-stage optimization process, where the shape of the cantilever and intrinsic topology features were adopted to enhance power. In the first stage, the notable increment doubled, while in the second stage, the increment was 11% higher, compared to a traditional rectangular cantilever. Wein et al. [14] incorporated stress constraints to optimize a harvester topologically. Their design has higher flexibility due to its varying shapes. High power capacity is achieved for structures at their resonance.

In shape and geometry optimization, optimum design shapes and geometric configurations are determined to maximize output power. Dietl and Garcia [15] sought to optimize the shape of a non-uniform width harvester. They intended to localize the strain in zones where it could yield the utmost power. A heuristic code was developed and utilized to obtain optimum shapes. Harvested power was found to increase in devices constrained by mass, and the mass was found to decrease in devices constrained by power. Similarly, Park et al. [16] optimized a rotary motion energy harvesting device. Well tapered and rectangular cantilevers were analyzed. The setup was simulated using Sequential Quadratic Programming, and a 37% energy increase was realized. On the other hand, Mohamed et al. [17] validated a new shape optimization technique. A range of shapes from rectangular to triangular, T-shaped, L-shaped, and variable-width shapes were optimized. It was inferred that the T-shape produced the highest power. Wang et al. [18] attempted to improve output from a harvester by the use of a double cantilever. A substantial improvement was realized.

Many optimization techniques have been developed and deployed. Shape and topology optimization are the most common, and they are well suited for single-mode harvesters. It is also challenging to envisage locations of high stress for piezoelectric material placement. Similarly, the use of prestressed beams or beams with an initial curvature reduces the amount of force under which the harvesters can operate effectively, as they encourage failure. If implemented in the multi-mode harvesters, these techniques affect the distribution of the fundamental frequencies, resulting in a large separation between them. This study aims to enhance the power output of a multimodal energy harvester through the selection of optimal geometrical parameters using the COMSOL Multiphysics optimization module. On the other hand, the end masses have been used for frequency tuning in the literature with no consideration of their effect on the power output. Therefore, this study attempts to determine the optimum magnitude of the end masses for maximum power output.

Finite Element Method (FEM) has been extensively used to accurately study vibration energy harvesters. Validation of the finite element method results has been achieved through either analytical methods [19, 20], or experimentally [21, 22]. Both these methods have shown that FEM can accurately and effectively study energy harvesting methods, and as a result, COMSOL FEM has been chosen for this study.

2. Harvester design

The harvester's design features a split cantilever multi-resonant energy harvester (SCMEH), as shown in Fig.1. The design presented by the authors in the un-optimized form [23] will be subject to optimization in this study.

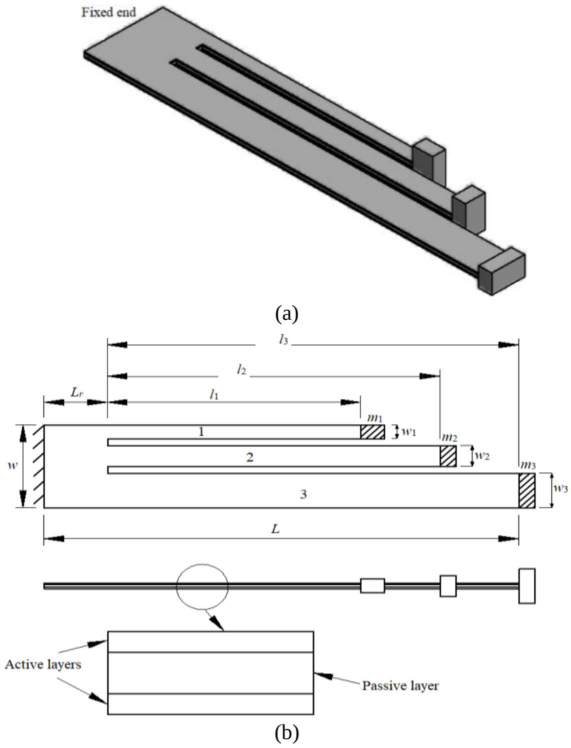

Figure 1. Schematic view of the proposed harvester:(a) Design of the SCMEH; and (b) detailed view.

The design constitutes a beam with two parallel splits to form branches of unequal length and width. The difference in width serves to lessen out-of-phase vibration of the branches, which may lead to voltage cancellation. On the other hand, the effect of the difference in length of the branches, on the other hand, aids in providing an appropriate distribution of natural frequencies. The piezoelectric layer is deposited on both sides of the substrate to form a bimorph. Each branch has a tip mass for tuning the fundamental frequencies of the harvester. The harvester's design is versatile since it can effortlessly be modified to suit target vibration sources, and thus it can be used in a wide range of applications. Furthermore, it requires low excitation forces as it is free of linkages, which makes it suitable for ambient environmental vibrations. The design minimizes phase differences and thereby achieves higher peak energy when compared to other designs explored in the literature, as well as produces high power density. The materials used for both the substrate and piezoelectric material of the harvester are shown in Table 1.

Table 1. Material properties of the harvester

Parameter	Substrate	Piezoelectric
Material	Brass	PZT-5H
Elastic modulus (GPa)	110	127
Poisson's ratio	0.33	0.31
Density(kg/m^3)	9000	7500

Brass is the preferred substrate material due to its high modulus, which supports a substantial magnitude of the tip masses without deflection. In addition, it can be applied in several vibration environments. Similarly, PZT-5H is the preferred piezoelectric material because of its higher piezoelectric constant.

3. Harvester parametric study

The parameters chosen for the harvester's optimization are the tip masses' magnitudes, the harvester's length, and the thicknesses of the substrate and piezoelectric materials. The effect of mass and length on natural frequencies was found and demonstrated in the previous work by the authors [23]. It was inferred that increasing beam length reduces the fundamental frequencies while increasing beam thickness increases the natural frequency. However, the effect of width on the natural frequency is relatively small[24], but the branch width significantly affects the phase variation in the vibration, as previously confirmed by the authors [23]. Therefore, proper selection of beam size parameters is essential to achieve a suitable design for a specified application. The initial parameters of the harvester, as obtained from the parametric study by the authors [23], are presented in Table 2.

Table 2. Parameters of the proposed SCMEH [23]

Parameter Symbol	Description	Substrate	PZT	Mass
L(mm)	Length	60	60	
L_r(mm)	Length of root	18	18	
w(mm)	Width	12	12	
w_1(mm)	Width of branch 1	2	2	
w_2(mm)	Width of branch 2	3	3	
w_3(mm)	Width of branch 3	5	5	
l_1(mm)	Length of branch 1	32	32	
l_2(mm)	Length of branch 2	42	42	
l_3(mm)	Length of branch 3	52	52	
t(mm)	Depth	0.4	0.2	
m_1(g)	Mass on branch 1			49
m_2(g)	Mass on branch 2			41
m_3(g)	Mass on branch 3			51

4. Modeling of the harvester

The harvester, being a mechanical system, is represented as a spring mass and damper system with the applied acceleration as a forcing function. Modeling the system as an inertial mass component under a base acceleration, its internal resistance analogizes the stiffness element. A damper is incorporated to analogize the energy dissipation.

For simplicity, the system is assumed to be a lumped mass model, and its coupled governing equations are written as:

$$m\ddot{z}+c\dot{z}+kz+\alpha v=m\ddot{y} \tag{1}$$

$$\frac{v}{R}+c_p\frac{dv}{dt}=\alpha\frac{dz}{dt} \tag{2}$$

where; $\ddot{z}=\ddot{x}-\ddot{y}$

α and c_p in Eq. (2) are defined as;

$$\alpha=\frac{eA}{L}$$

$$c_p=\varepsilon^s\frac{A}{L} \tag{3}$$

where $\dot{z}$ and z are the relative velocity and displacement vector tensors respectively. Eq. (3) depicts the influence of harvester parameters on piezoelectric constants.

Eq. (1) represents the mechanical part of the system, while Eq. (2) represents the electrical part. A combination of the two is known as electromechanical coupling [26]. On the other hand, the following equations govern the piezoelectric effect:

$$\{s\}=\left[s^E\right]\{T\}+\left[d^t\right]\{E\} \tag{4}$$

$$\{D\}=[d]\{T\}+\left[\varepsilon^T\right]\{E\} \tag{5}$$

Equations (4) and (5) express the inverse and direct piezoelectric effects, respectively. Since the system is under the direct piezoelectric effect, Eq. (5) is used to describe it, whereby the induction of stress in the beam leads to the production of charge.

The constants in Eq. (4) show the influence of individual harvester parameters on the harvester's performance. The above model is solved as a distributed model using the Finite Element Method (FEM) in COMSOL Multiphysics to determine its response.

4.1. Optimization formulation

The finite element model of the design described above is modeled in COMSOL Multiphysics. Through a grid-independent test, a range of element sizes ranging from coarse to extremely fine were tested and their effects analyzed. The element size is selected such that the accuracy of the solution is not dependent on it while maintaining a reasonable computational time. Hence, a fine size was used in this study and skewness was used to test for the element quality. A natural frequency study was conducted to determine its eigen frequencies. In the frequency domain study, the optimization module is applied. BOBYQA (Bound Optimization BY Quadratic Approximation) is chosen as the optimization solver due to its robustness and numerous advantages as described by Powell [27]. BOBYQA is an iterative algorithm to optimize any function, with each iteration employing a quadratic approximation. The medians of the bounds are selected as the initial values to reduce the computational effort when seeking the optimal values. Since BOBYQA is bound-constrained, no derivatives are provided by the user, and for this reason, extreme geometric parameter values related to the objective can be executed.

The output power (P) of the harvester is selected as the design objective function and it is defined as:

$$P=I_0V_0=I_0^2R \tag{6}$$

Where I_0 and V_0 are the output current of the harvester and the voltage drop, respectively, at the initial load resistance ($R=10k\Omega$). The relationship between the harvester output power and the device parameters is illustrated by α and c_p in Eq. (3), whereas the relationship between the mechanical strain and piezoelectricity is shown in Eqs. (4) and (5).

By incorporating the terms in Eq. (3) the objective function as derived by Lefeuvre et al.[28] becomes:

$$P=V_{rec}\left(\frac{2\alpha}{\frac{\pi}{2}+Rc_p\omega}+c_v\frac{\frac{\pi}{2}+Rc_p\omega}{\alpha R}\right) \tag{7}$$

To illustrate the effect of the respective harvester parameters on the power output, the constituent terms of Eq. (3) are substituted in Eq. (7) yields the following equation:

$$P=V_{rec}\left(\frac{2eA}{\frac{\pi L}{R}+R\omega A\varepsilon^s}+c_v\frac{\frac{\pi L}{2}+R\omega A\varepsilon^s}{2eAR}\right) \tag{8}$$

In Eq. (8), the length L represents all the aspects of length l_1, l_2, and l_3. On the other hand, all the mass elements m_1, m_2, and m_3 are illustrated since the natural frequency depends on the inertial component of mass.

Since $V_{rec} = \frac{V_0}{\sqrt{2}}$,

Therefore, the objective function is

$$P = \frac{(V_0)^2}{2R} \quad (9)$$

With the objective function now setas Eq. (9), the control variables can be expressed as the lower and upper bounds of the design parameters shown in Table 3, while the constraint, which is the natural frequency of the vibration, is expressed as:

$$g_1 \leq 17Hz \quad (10)$$

The 17 Hz constraint is chosen to accommodate any deviation that may ensue due to the changes in dimensions and mass magnitudes after the optimization process, as the structure, in its unoptimized form, was initially designed to perform at a frequency below 15 Hz.

Table 3. control variables

parameter	Lower bound	Upper bound
l_1(mm)	10	60
l_2(mm)	10	60
l_3(mm)	10	60
t_1(mm)	0.1	0.5
t_2(mm)	0.1	0.5
m_1(g)	5	60
m_2(g)	5	60
m_3(g)	5	60

The objective function in Eq. 9 and the control variables in Table 3 are applied in the optimization module, and the BOBYQA algorithm generates optimal parameters for the harvester. The fixed values of the design parameters represent the bounds around which the algorithm attempts to find the values that yield the maximum power. The upper bound was selected as the longest permissible length under which the structure could operate without initial curvature occurring, while the lower bound was chosen arbitrary to a length under which no notable deflection could happen with the available loading. The optimization procedure is shown in Fig. 2. A COMSOL FE model is used to compute the performance required for optimization. Power and mechanical stress are two examples. The optimal values obtained are shown in Table 4.

Table 4. Optimum parameters of the harvester

parameter	Optimal value
l_1(mm)	27.704
l_2(mm)	36.886
l_3(mm)	51.224
t_1(mm)	0.44015
t_2(mm)	0.20402
m_1(g)	49.0846
m_2(g)	41.5765
m_3(g)	51.975

The parameters for the optimal harvester presented in Table 4 are used to simulate the optimized SCMEH, and to determine its performance which will be discussed in the coming section.

5. Simulation of the optimized harvester

The optimized harvester is modeled in COMSOL Multiphysics using the optimal parameters obtained from optimization shown in Table 4. Boundary conditions are applied to the harvester to simulate its response. The boundary conditions include a base acceleration of 0.2 g and a load resistance of 10 kΩ. The resistance is chosen to emulate an open circuit state. The condition that must be satisfied by the resistance is that it must be greater than the internal resistance of the piezoelectric material. However, later in this work, an optimum resistance for maximum power output will be evaluated. A damping loss factor of 0.001 is selected for damping. The loss factor is selected according to the material properties, as provided in the COMSOL material library. The initial displacement is zero, and the ground and terminals are configured to assume a parallel connection. An eigenfrequency study was first conducted to obtain the mode shapes and the fundamental frequencies that need to be matched to the source frequency for the harvester to operate at its resonant frequencies.

5.1. Eigenfrequency study

The optimized harvester's mode shapes are shown in Figure 3. The first, second, and third fundamental frequencies are 11.729 Hz, 13.951 Hz, and 15.36 Hz. In the harvester's unoptimized form, the first, second, and third natural frequencies are10.702 Hz, 12.702Hz, and 14.007Hz, respectively. This signifies a slight variation in the natural frequency. However, the variation is within the targeted value of ≤17Hz. The variation in the magnitude of the natural frequencies is due to the change in harvester dimensions brought about by optimization. In the first mode shape, Fig. 3(a), all the branches deflect in the same direction, with branch 3 having the maximum deflection. No phase difference is experienced; hence maximum strain is induced on the piezoelectric element, since torsional vibration is minimal. During this mode, the highest peak power is expected since no voltage cancellation effect exists. Branches 1 and 2 deflect in the same direction in the second mode, while branch 3 deflects slightly in the opposite direction resulting in a slightout-of-phase vibration as illustrated in Fig. 3 (b). For this reason, the expected voltage and power peaks will be somewhat lower than the voltage and power in the first mode. During the third mode, shown in Fig. 3 (c), branches 1 and 2 deflect in opposite directions, while branch 3 remains undeflected. Such deflection results in a large out-of-phase vibration, and the lowest power peak is expected in this mode. This is due to the cancellation effect of the power and voltage peaks in the bending modes. The cancellation arises because part of the beam is under tension while the other part is under compression to produce a torsional effect. The energy from the torsional modes is not considered in this study.

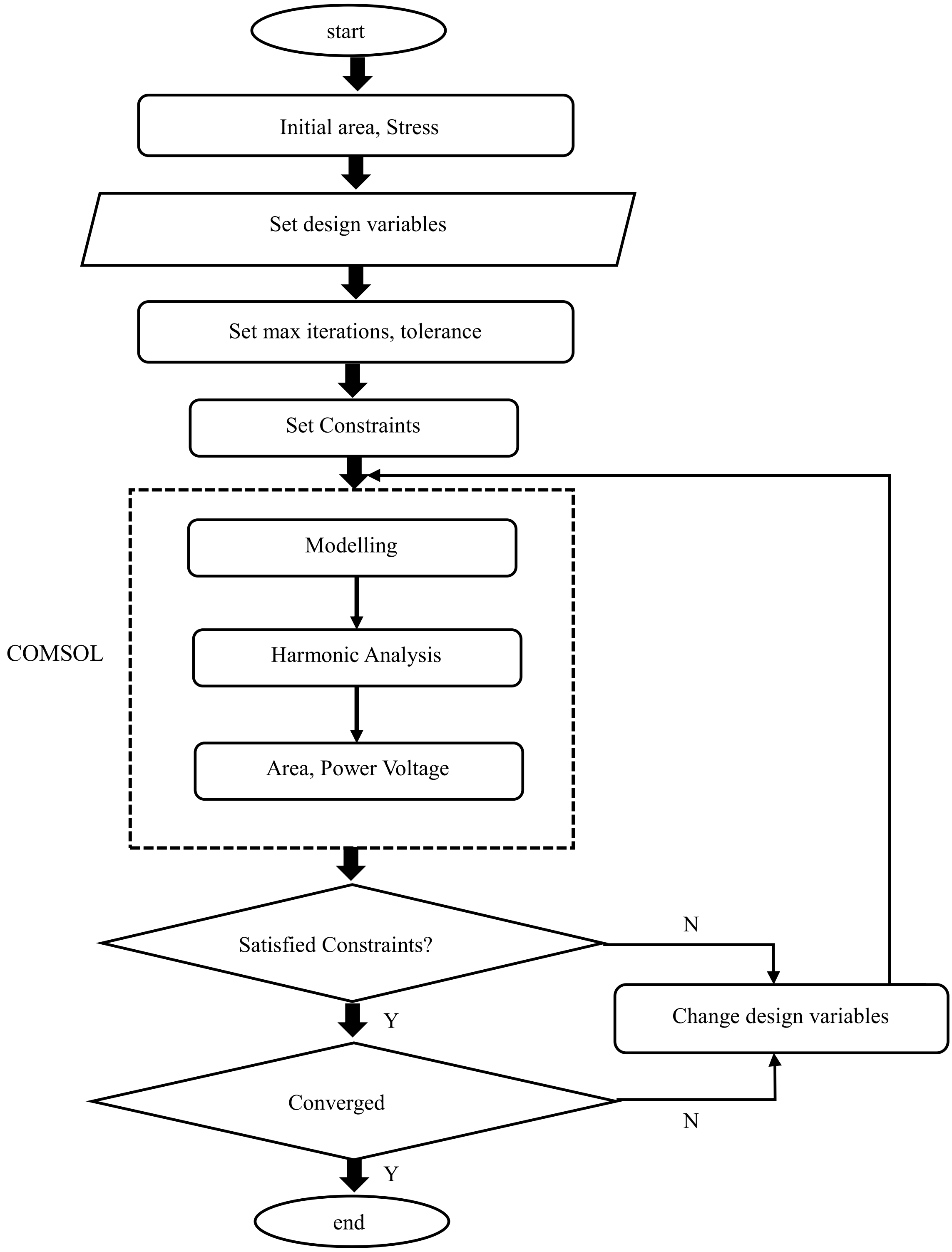

Figure 2. Procedure for COMSOL Optimization process

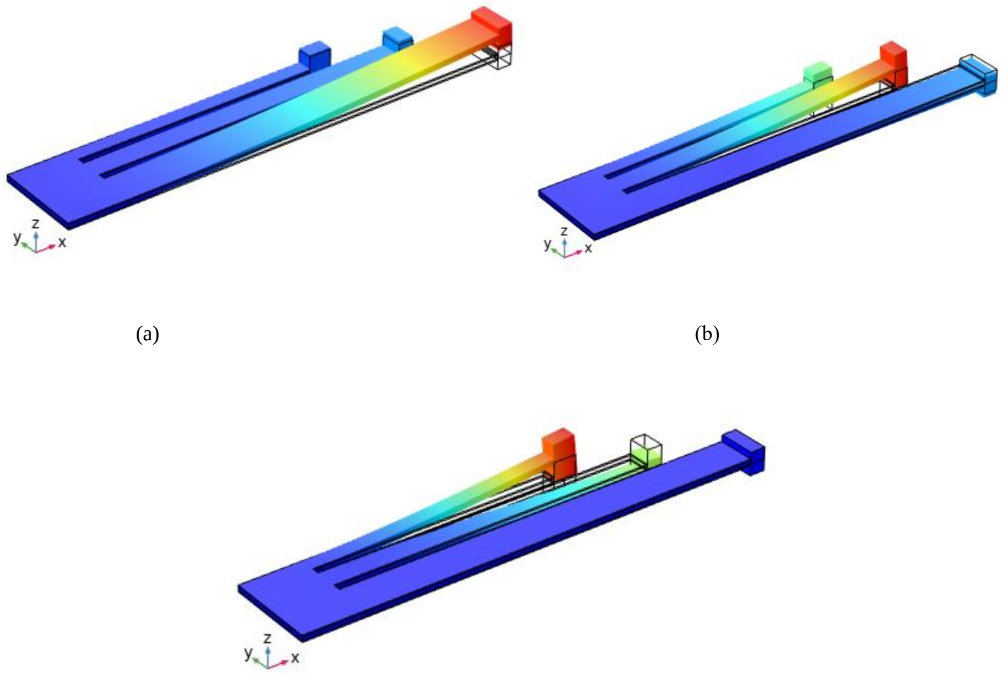

(a) (b)

(c)

Figure 3. Eigen frequencies and mode shapes of the harvester: (a) 1stmode shape, (b) 2ndmode shape and (c) 3rd mode shape

5.2. Frequency response of the harvester

A harmonic analysis is conducted to determine the response of the harvester in the frequency domain and to verify the natural frequencies obtained from the modal analysis. The boundary conditions under which the study is carried out include a base acceleration of 0.2g, a resistance of 10 $k\Omega$, initial displacement of zero, and a damping loss factor of 0.001. The criteria for selecting the resistance and the damping factor are stated in the previous section. A frequency sweep is carried out at a frequency range between 9.5Hz and16.5Hz, and the response of the harvester is observed.

Figure 4 illustrates the frequency response of the harvester in both the unoptimized and optimized states. The dashed line represents the response of the unoptimized state, while the solid line represents the optimized state. The response is highlighted in terms of voltage and power. Fig. 4 (a) shows the voltage drop across the piezoelectric element due to the vibration-induced piezoelectric effect. For the unoptimized state, the voltage values obtained are 65.11 V, 37.41 V, and 15.32V at the first, second, and third resonant frequencies, respectively. The natural frequencies corresponding to the voltage peaks are 10.25 Hz, 12.60 Hz, and 14.01 Hz.

On the other hand, the optimized harvester has three voltage peaks corresponding to the open circuit resonant frequencies. The first, second, and third resonant frequencies are 11.2 Hz, 13.8 Hz, and 15.4 Hz. The voltage magnitude values corresponding to these frequencies are 68.55 V, 53.33 V, and 14.24 V, respectively. It is worth noting that there is a slight variation between the natural frequencies obtained from modal analysis and harmonic analysis. The alteration of the harvester stiffness due to induced electrical damping brings about this variation in frequency. A comparison between the optimized and unoptimized states of the harvester shows a sufficient improvement through optimization. A notable increment of 15.41% in average voltage was realized compared to the prior unoptimized harvester. The maximum increment of 42.55% is observed in the second mode due to the reduced phase difference, which in turn reduces the voltage cancellation effect. The cancellation is prominent in the unoptimized harvester. However, the cancellation is high in the third mode due to a large out of phase variation.The variation leads to a slight reduction in the peak voltage. The reduction in voltagedoes not affect the overall improvement of the harvester's performance since the third peak is generally lower than the first two peaks. A notable drop in voltage and power is seen between the first and second resonant peaks of the unoptimized harvester at 12Hz. The decline is caused by the antiresonance phenomenon [25].The 12Hz frequency is the antiresonance frequency, whereby the vibration amplitude drops to almost zero. Even though the performance is improved after optimization, the antiresonance effect is still visible at 13.1 Hz, which is a prevalent occurrence in multi-degree of freedom systems, particularly those under direct excitation [29]. Fig.4(b) shows the power generated across the 10kΩ resistor.As shown by the dashed line, the power peak power values of the unoptimized harvester are 212.8 mW, 69.95 mW, and 11.73 mW, corresponding to the first, second, and third resonant frequencies, respectively. For the optimized harvester, the three power peaks conforming to the first three resonant frequencies are 235.02 mW, 142.2 mW, and 10.15 mW, respectively, illustrated by the solid line. The utmost peak power increase is obtained in the second mode, with a rise of 74.52%. The average power increase across all the modes is 31.67%. The harvested power shows similar behavior to the voltage drop, except that the power is mainly dependent on the impedance. The relationship between the harvested power and the voltage is $\frac{v^2}{2R}$.The dependence of the harvested power on the impedance indicates that there exists a critical value of impedance upon which the harvested power is maximum and will be determined in the next section.

5.3. Performance at optimal resistance

A load dependence analysis in the frequency domain was undertaken to select the optimal resistance to generate maximum power. Theoretically, the tip deflection is minimum at a load resistance of $R = \frac{1}{2\omega c_p}$ where ω is the vibration frequency in rad/s. This propounds that for improved performance, the resistance should be set at a critical value. It is noted that very high or very low impedance has a detrimental impact on the harvester's power or voltage magnitude [31, 32].

Fig.5 illustrates the response of the optimized and unoptimized states of the SCMEH at their respective optimal load resistances. The response of the optimized harvester is plotted by the dashed line, while the solid line plots that of the unoptimized harvester. It is worth noting that each mode has its own load value where maximum power can be harvested. Therefore, the optimum load is considered to be at the first peak, where the output power of the harvester is generally higher and can compensate for the subsequent modes. For the optimized harvester, the optimal load resistance obtained from the load dependence study is 1.778 kΩ, whereby a peak power of 416.8 mW is realized in the first mode, as shown in Fig.5(a).

On the other hand, the optimal resistance of the unoptimized harvester is 5.62 kΩ, with a peak power of 220.1 mW in the first mode. When comparing the performance of the SCMEH in both the optimized and unoptimized states, an 89% power increase is achieved in the first mode. On average, a power increase of 56% is realized across all resonant peaks of the optimized harvester compared to the unoptimized one. The optimized harvester is thus more efficient since the optimum load is lower than that of the unoptimized state. The capability of the harvester to operate at a low impedance eliminates the need to use infinitely large loads as previously employed in the literature. The advantage of lowering optimal loads is that sufficiently high power values can be obtained without sacrificing the voltage magnitudes, which yields relatively high voltages while minimizing the power output. Fig.5(b) shows the relationship between load magnitudes and the voltage drop in the two states of the harvester. In both states, the voltage increases to an asymptotic value with an increase in load resistance. However, at a specific value of the load, the effect of the load diminishes. This further explains the need for an optimal resistance value since any further increase in load will adversely affect the power output. The voltage values in the optimized state are generally higher than those in the unoptimized states.

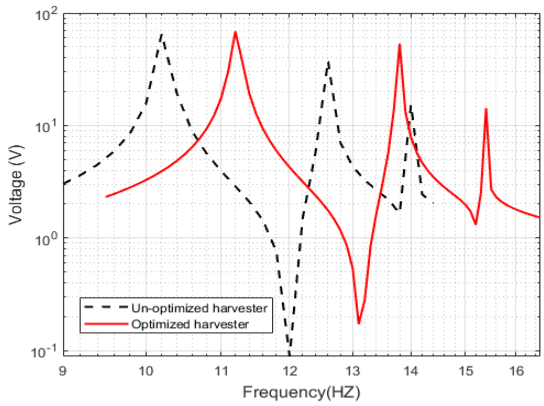

(a)

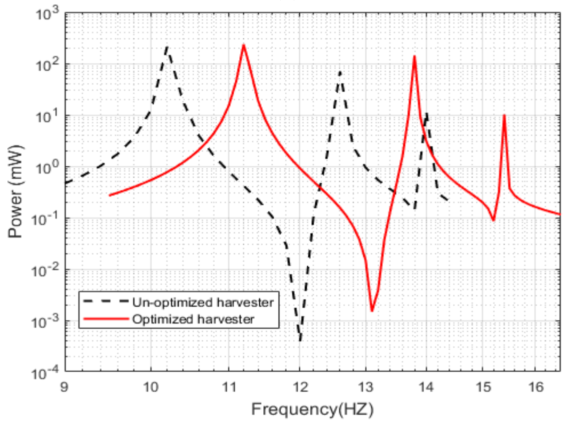

(b)

Figure 4. Frequency response of the harvester : (a)voltage and (b) power

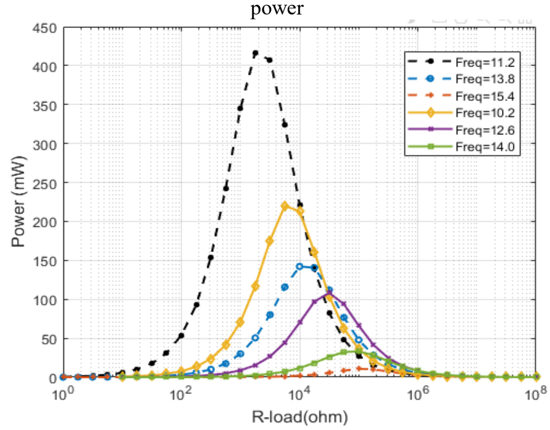

(a)

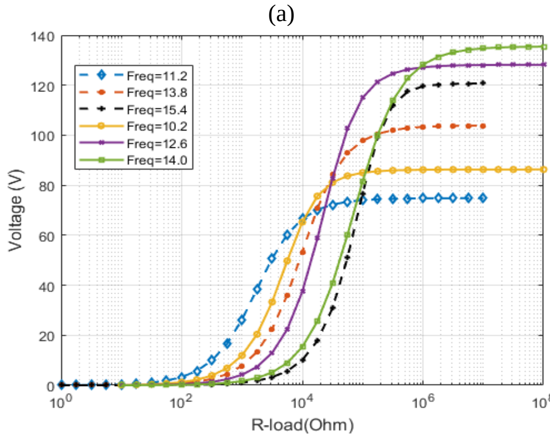

(b)

Figure 5. Performance under varying load resistance: (a) power and; (b) voltage

5.4. Performance under varying acceleration

It is logical to predict that as acceleration values increase,so will the performance of both harvesters. However, the proportion of the increase is unknown, and therefore, this analysis seeks to understand the relationship between acceleration and harvester performance.

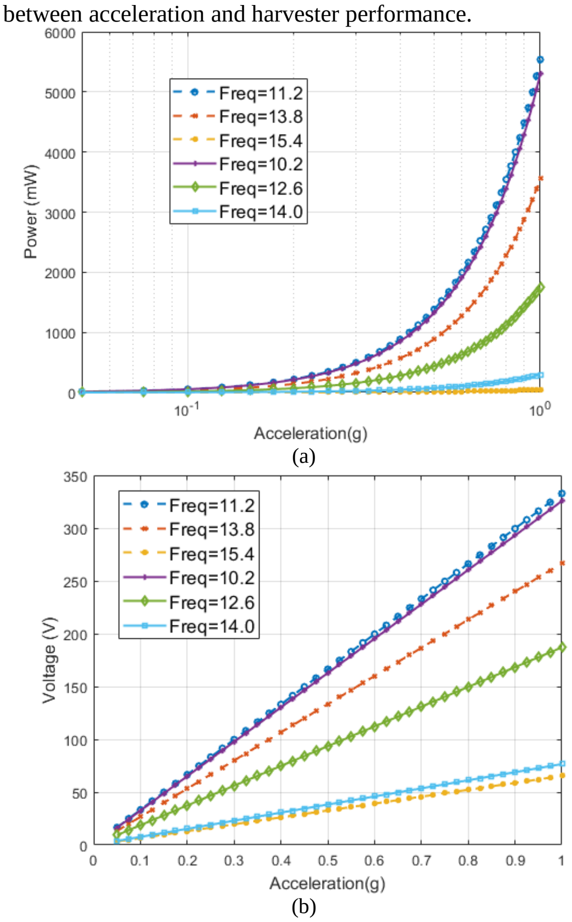

Figure 6. Performance under varying acceleration: (a) power and; (b) voltage

Figure 6 illustrates the influence of acceleration on both the optimized and unoptimized states of the SCMEH. The dashed line shows the performance of the optimized state, while the solid line shows the performance of the unoptimized state. Usually, the performance of any given harvester largely depends on the magnitude of force applied through acceleration. This force, however, should be limited to the factor of safety of the harvester's materials to avoid damage or singularity [33]. The harvested power for optimized and unoptimized states varies exponentially with the applied base acceleration, as shown in Fig. 6 (a).On the other hand, the voltage varies linearly with the base acceleration, as shown in Fig. 6 (b). Under the same acceleration values, the average power and voltage trend indicate that the optimized state has higher magnitudes, unlike the unoptimized one. This shows that more energy levels can be harvested with the optimized state even when lower excitation forces are used. However, acceleration may give a false impression if solely used as the only factor to enhance the harvester's performance. This is because, beyond critical strain values, no more strain can be induced in the material, provided yield stress is not exceeded.

6. Influence of individual material proportions on the performance of the harvester

The proportions of both the piezoelectric and substrate materials tend to affect the frequency and performance of the harvester [9]. This has been brought to light by the volume difference between the optimized and unoptimized harvesters. The un-optimized harvester has a 50% proportion of the substrate and piezoelectric materials, whereas the optimized one has 48%of the piezoelectric material and 52% of the substrate material. Therefore, a study was carried out on the optimized harvester to empirically determine the effect of material proportions on the harvester's performance. Since the length and breadth of both materials are identical, a sweep of the material depths will be used to study this variation. However, during the study of this variation, the volume of the harvester was kept constant. This is achieved by varying the material thickness and not limiting the variation to the piezoelectric material.

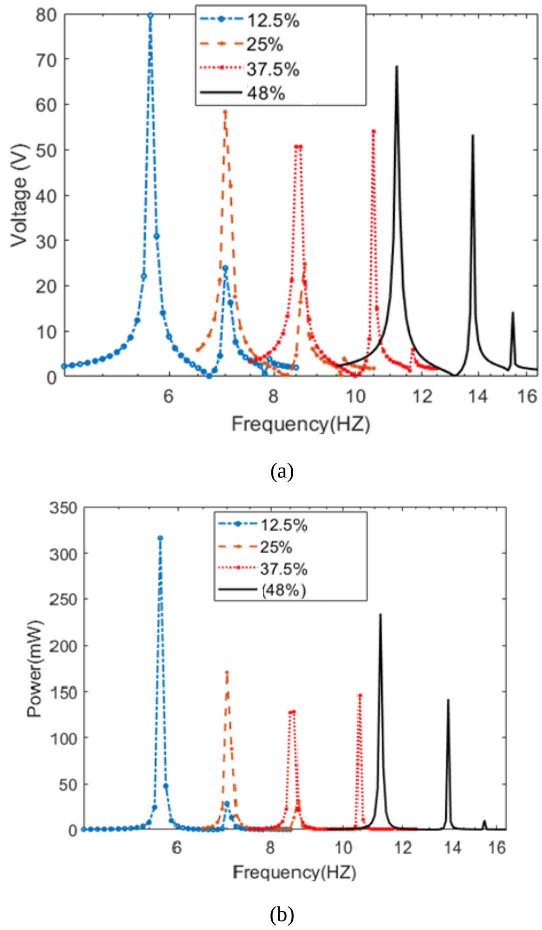

Figure 7. Effect of varying piezoelectric proportion percentage below the optimum: (a) voltage and; (b) power

Figure 7 shows the harvester's performance with various values of the piezoelectric material depth below the optimum depth. The material is varied from 0.05mm to 2mm at an interval of 0.05 mm, which translates to a proportion of 12.5% to 37.5% at a 12.5% interval of the total volume of the harvester. At 12.5%, the first mode peak is the highest, at 79*V*, but with a little noise as its value rises towards the peak. The second and third modes are relatively lower compared to the corresponding modes of other proportions. At the 25% piezoelectric proportion, the voltage is somewhat higher atthe first peak, at 59*V*, while the subsequent modes' peaks diminish significantly with some noise as the vibration transitions from the first peak to the second peak. At a 37.5% piezoelectric proportion,the first and second mode voltage peaks tend to have the same magnitude of about 54*V*. Their distribution is reasonably good, but the first mode terminates at the beating frequency before resonance is reached.In addition, in the first mode, the vibration changes direction before fully equalling the natural frequency of the harvester.Therefore, it does not have a distinct peak, and for this reason, this piezoelectric proportion is not appropriate for use in the SCMEH. At the optimal design, where the piezoelectric proportion is 48%, improved performance is realized.Sufficiently higher voltages of 69.95 *V*, 53.3 *V*, and 11.73*V* are obtained in the first, second, and third modes.

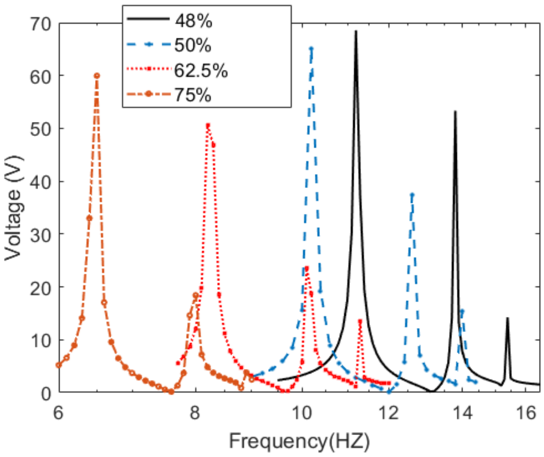

(a)

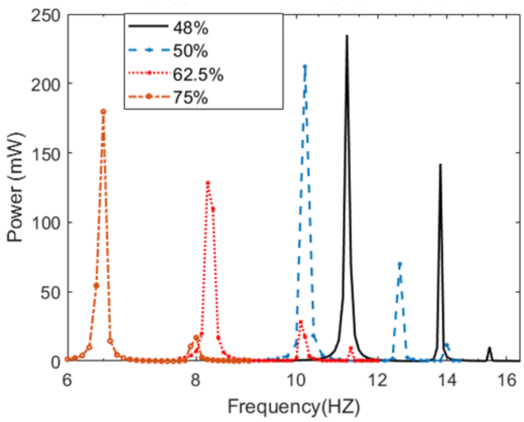

(b)

Figure 8. Effect of varying piezoelectric proportion percentage above the optimum: (a) voltage and; (b) power

Figure 8 illustrates the harvester's performance under varied substrate material depths. Since the substrate thickness is varied, the piezoelectric depth is above the optimum value. When the piezoelectric proportion is above the optimum, it has a significant effect on the harvester's performances well as the overall strength and integrity of the device. This, in turn, translates into the service life of the harvester. Therefore, it is not recommended to design the harvester with the 87.5% and 75% piezoelectric proportions because the depth of the substrate is significantly reduced, and initial curvature may occur before excitation. However, the 75% piezoelectric proportion has been included in this study to examine the behavioral response but not for operational purposes. As shown in Fig. 8 (a), the peak voltages are 59.95 *V* and 18.4 *V*for the 75% proportion. On the other hand, the 62.5% piezoelectric material proportion has a voltage of 50*V* in the first mode, with some noise immediately after the peak. The voltages in the second and third modes are 23.56 V and 13.48 V, respectively. At the50% piezoelectric proportion, a fair distribution of voltage peaks is shown, with 65.1 *V*, 36.2 *V*, and 13.6 *V* in the first, second, and third modes, making it a reasonably good design for this harvester. Nevertheless,compared to the optimized form, all the other proportions have a relatively lower output power, rendering the optimal design efficient.Moreover, the power generated is proportional to the voltage when the load resistance is maintained at a constant relationship as presented in Eq. (9). Therefore, a considerable improvement is experienced in the optimal design in terms of power and noise elimination. It is inferred that high performance is achieved when the piezoelectric material is slightly lower at 46% to 48% of the harvester's total volume. The changing piezoelectric coupling coefficient brings about differences in the harvester's performance with various piezoelectric proportions in the piezoelectric material. Furthermore, the mass element affects performance because performance is heavily dependent on the inertial component. However, with large thickness values of the substrate, the performance tends to decrease since high excitation forces are required to induce reasonable strain, as the internal resistance of the substrate resists deformation. The power values in both figures7 and 8 are proportional to the voltage. The proportionality is similar to that illustrated in section 5.2.

7. Comparison to a Multi-Resonant Energy Harvester (MRPEH)

The performance of an optimized SCMEH is compared to that of an experimentally validated Multi-Resonant Piezoelectric Energy Harvester (MRPEH) [34]. The MRPEH features two triangular branches on the main beam and a Macro-Fiber Carbon (MFC), a piezoelectric element. The MPEH's base is excited with a 0.2 g base acceleration and a 1 MΩ load connected across its terminals. Two resonant peaks are obtained at the frequencies of 3.89 Hz and 7.81 Hz, at which a voltage of 21.69 V and 9.3 V, respectively, is shown in Fig. 9(a).

The power comparison, on the other hand, shows a greater disparity. Because it can perform efficiently at low impedance values, the SCMEH achieves superior peak values as shown in Fig. 9(b). For this reason, at its optimal impedance of 1.778 kΩ, the maximum peak obtained is 416.8 mW.

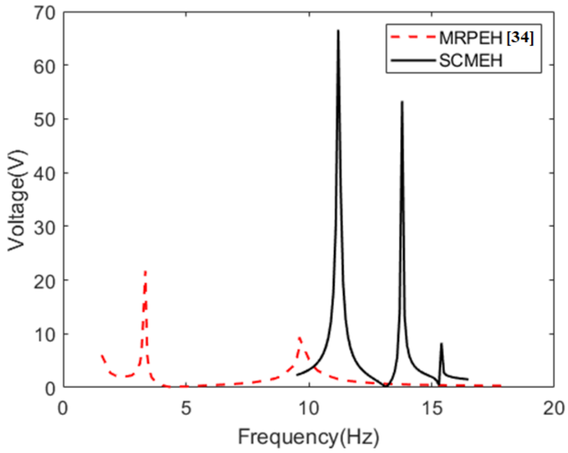

(a)

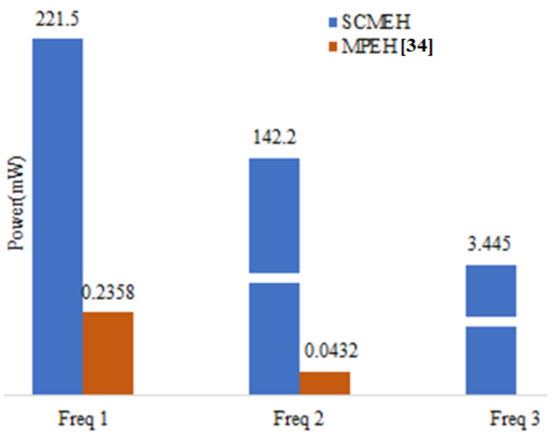

(b)

Figure 9. Performance comparison between SCMEH and MRPEH [34]: (a) voltage and (b) power

Conclusion

The optimized multimodal harvester in this study provides an insight into an optimization technique to optimize a multimodal harvester without using sensors or complex algorithms. In the literature, the magnitudes of the end masses and harvester lengths have been used to tune the resonant frequencies but not to enhance performance and output. However, in this work, masses and lengths have been used to influence the output power. The efficiency of the optimized harvester is reflected by high output power and superior power density (power per unit volume) compared to the unoptimized harvester. The proposed dimensional optimization technique showed that using 48% of the piezoelectric proportion for this harvester and 52% substrate proportion yields the maximum power. Also, the load resistance was reduced from 5.62kΩ in the unoptimized harvester to 1.778kΩ, and this is an advantage since unmatched impedance leads to power loss. It is also realized that the effective mass of the harvester was reduced, which increases its applicability, as it can be retrofitted in many additional different areas. By increasing the acceleration values, the output of the optimized harvester increases. However, acceleration cannot indicate better performance since, at practically higher values, the harvester materials may yield. Generally, through optimization, the average power output increased by 31.67% at 0.2g acceleration and 10kΩ load resistance. With the high rate of adoption of IoT and wireless sensor networks in structures, the development of highly efficient energy harvesters will aid in the continuity of their operation. Therefore, the harvester proposed in this study is deemed to offer a solution to the intermittency experienced in the operations of microelectronic devices during battery replacements. Further incorporation of active frequency tuning mechanisms can be explored for the proposed multimodal harvester in the future.

Conflict of interest

The authors declare that there is no conflict of interest regarding this submission.

References

[1] V. S. Gaikwad and S. S. Chinchanikar, “Adaptive Neuro Fuzzy Inference System to Predict the Mechanical Properties of Friction Stir Welded AA7075-T651 Joints,” *Jordan Journal of Mechanical and Industrial Engineering,* vol. 16, no. 3, pp. 381–393, 2022.

[2] J. Lange, J. Hilgedieck, and M. Kaltschmitt, “Renewable resources of energy for electricity generation-development trends and necessities within the overall energy system,” *Jordan Journal of Mechanical and Industrial Engineering*, vol. 13, no. 3, pp. 207–220, 2019.

[3] E. J. Majeed and A. J. Majeed, “Harvesting Human Being Energy to Charge Smartphone,” *Jordan Journal of Mechanical and Industrial Engineering*, vol. 16, no. 3, pp. 439–448, 2022.

[4] M. M. Ahmad, N. M. Khan, and F. U. Khan, “Multi-degrees of freedom energy harvesting for broad-band vibration frequency range: A review,” *Sensors Actuators A Phys.*, vol. 344, no. June, 2022, doi: 10.1016/j.sna.2022.113690.

[5] J. Cho, M. Anderson, R. Richards, D. Bahr, and C. Richards, “Optimization of electromechanical coupling for a thin-film PZT membrane: II. Experiment,” *J. Micromechanics Microengineering*, vol. 15, no. 10, pp. 1804–1809, 2005, doi: 10.1088/0960-1317/15/10/003.

[6] Q. Wang and N. Wu, “Optimal design of a piezoelectric coupled beam for power harvesting,” *Smart Mater. Struct.*, vol. 21, no. 8, 2012, doi: 10.1088/0964-1726/21/8/085013.

[7] H. S. Yoon, G. Washington, and A. Danak, “Modeling, optimization, and design of efficient initially curved piezoceramic unimorphs for energy harvesting applications,” *J. Intell. Mater. Syst. Struct.*, vol. 16, no. 10, pp. 877–888, 2005, doi: 10.1177/1045389X05055759.

[8] H. Elahi, “The investigation on structural health monitoring of aerospace structures via piezoelectric aeroelastic energy harvesting,” *Microsyst. Technol.*, vol. 27, no. 7, pp. 2605–2613, 2021, doi: 10.1007/s00542-020-05017-y.

[9] Elahi, H.; Rizwan Mughal, M.; Eugeni, M.; Qayyum, F.; Israr, A.; Ali, A.; Munir, K.; Praks, J.; Gaudenzi, P. Characterization and Implementation of a Piezoelectric Energy Harvester Configuration: Analytical, Numerical and Experimental Approach. In-tegr. Ferroelectr. 2020, 212, 39–60.10.1080/10584587.2020.1819034.

[10] G. Acciani, A. Dimucci, and L. Lorusso, “Multimodal piezoelectric devices optimization for energy harvesting,” *Int. J. Multiphys.*, vol. 7, no. 3, pp. 227–243, 2013, doi: 10.1260/1750-9548.7.3.167.

[11] C. Kim and J. W. Shin, “Topology optimization of piezoelectric materials and application to the cantilever beams for vibration energy harvesting,” *Int. J. Precis. Eng. Manuf.*,

vol. 14, no. 11, pp. 1925–1931, 2013, doi: 10.1007/s12541-013-0261-1.

[12] S. Lee and A. Tovar, "Topology optimization of piezoelectric energy harvesting skin using hybrid cellular automata," *J. Mech. Des. Trans. ASME*, vol. 135, no. 3, pp. 1–11, 2013, doi: 10.1115/1.4023322.

[13] C. K. Thein and J. S. Liu, "Numerical modeling of shape and topology optimisation of a piezoelectric cantilever beam in an energy-harvesting sensor," *Eng. Comput.*, vol. 33, no. 1, pp. 137–148, 2017, doi: 10.1007/s00366-016-0460-3.

[14] F. Wein, M. Kaltenbacher, and M. Stingl, "Topology optimization of a cantilevered piezoelectric energy harvester using stress norm constraints," *Struct. Multidiscip. Optim.*, vol. 48, no. 1, pp. 173–185, 2013, doi: 10.1007/s00158-013-0889-6.

[15] J. M. Dietl and E. Garcia, "Beam shape optimization for power harvesting," *J. Intell. Mater. Syst. Struct.*, vol. 21, no. 6, pp. 633–646, 2010, doi: 10.1177/1045389X10365094.

[16] J. Park, S. Lee, and B. M. Kwak, "Design optimization of piezoelectric energy harvester subject to tip excitation," *J. Mech. Sci. Technol.*, vol. 26, no. 1, pp. 137–143, 2012, doi: 10.1007/s12206-011-0910-1.

[17] K. Mohamed, H. Elgamal, and S. A. Kouritem, "An experimental validation of a new shape optimization technique for piezoelectric harvesting cantilever beams," *Alexandria Eng. J.*, vol. 60, no. 1, pp. 1751–1766, 2021, doi: 10.1016/j.aej.2020.11.024.

[18] J. Wang, B. Fan, J. Fang, J. Zhao, and C. Li, "A Piezoelectric Energy Harvester Based on Multi-Cantilevers and Magnetic Force," *SSRN Electron. J.*, pp. 1–11, 2022, doi: 10.2139/ssrn.4153197.

[19] Z. Q. Lu, J. Chen, H. Ding, and L. Q. Chen, "Two-span piezoelectric beam energy harvesting," *Int. J. Mech. Sci.*, vol. 175, no. February, 2020, doi: 10.1016/j.ijmecsci.2020.105532.

[20] L. Tang and Y. Yang, "A multiple-degree-of-freedom piezoelectric energy harvesting model," *J. Intell. Mater. Syst. Struct.*, vol. 23, no. 14, pp. 1631–1647, 2012, doi: 10.1177/1045389X12449920.

[21] P. Panthongsy, D. Isarakorn, T. Sudhawiyangkul, and S. Nundrakwang, "Piezoelectric energy harvesting from machine vibrations for wireless sensor system," *ECTI-CON 2015 - 2015 12th Int. Conf. Electr. Eng. Comput. Telecommun. Inf. Technol.*, 2015, doi: 10.1109/ECTICon.2015.7207051.

[22] O. Rubes, M. Brablc, and Z. Hadas, "Nonlinear vibration energy harvester: Design and oscillating stability analyses," *Mech. Syst. Signal Process.*, vol. 125, pp. 170–184, 2019, doi: 10.1016/j.ymssp.2018.07.016.

[23] D. O. Masara, H. El Gamal, and O. Mokhiamar, "Split Cantilever Multi-Resonant Piezoelectric Energy Harvester for Low-Frequency Application," Energies, vol. 14, no. 16, p. 5077, Aug. 2021, doi: 10.3390/en14165077.

[24] K. Mohamed, H. Elgamal, and S. A. Kouritem, "An experimental validation of a new shape optimization technique for piezoelectric harvesting cantilever beams," *Alexandria Eng. J.*, vol. 60, no. 1, pp. 1751–1766, 2021, doi: 10.1016/j.aej.2020.11.024.

[25] D. Upadrashta and Y. Yang, "Trident-Shaped Multimodal Piezoelectric Energy Harvester," *J. Aerosp. Eng.*, vol. 31, no. 5, p. 04018070, 2018, doi: 10.1061/(asce)as.1943-5525.0000899.

[26] Q. Wang, W. Dai, S. Li, J. A. S. Oh, and T. Wu, "Modelling and analysis of a piezoelectric unimorph cantilever for energy harvesting application," *Mater. Technol.*, vol. 35, no. 9–10, pp. 675–681, 2020, doi: 10.1080/10667857.2020.1751470.

[27] M. Powell, "The BOBYQA algorithm for bound constrained optimization without derivatives," *NA Rep. NA2009/06*, p. 39, 2009, [Online]. Available: http://www6.cityu.edu.hk/rcms/publications/preprint26.pdf.

[28] E. Lefeuvre, D. Audigier, C. Richard, and D. Guyomar, "Buck-boost converter for sensorless power optimization of piezoelectric energy harvester," *IEEE Trans. Power Electron.*, vol. 22, no. 5, pp. 2018–2025, 2007, doi: 10.1109/TPEL.2007.904230.

[29] J. Welte, T. J. Kniffka, and H. Ecker, "Parametric excitation in a two degree of freedom MEMS system," *Shock Vib.*, vol. 20, no. 6, pp. 1113–1124, 2013, doi: 10.3233/SAV-130826.

[30] E. L. B. Van De Vorst, D. H. Van Campen, A. De Kraker, and R. H. B. Fey, "Periodic solutions of a multi-DOF beam system with impact," *J. Sound Vib.*, vol. 192, no. 5, pp. 913–925, 1996, doi: 10.1006/jsvi.1996.0225.

[31] J. Liang and W.-H. Liao, "Impedance matching for improving piezoelectric energy harvesting systems," *Act. Passiv. Smart Struct. Integr. Syst. 2010*, vol. 7643, no. 852, p. 76430K, 2010, doi: 10.1117/12.847524.

[32] A. Koszewnik, P. Grześ, and W. Walendziuk, "Mechanical and electrical impedance matching in a piezoelectric beam for Energy Harvesting," *Eur. Phys. J. Spec. Top.*, vol. 224, no. 14–15, pp. 2719–2731, 2015, doi: 10.1140/epjst/e2015-02585-5.

[33] X. D. Xie, A. Carpinteri, and Q. Wang, "A theoretical model for a piezoelectric energy harvester with a tapered shape," *Eng. Struct.*, vol. 144, pp. 19–25, 2017, doi: 10.1016/j.engstruct.2017.04.050.

[34] I. Izadgoshasb, Y. Y. Lim, R. V. Padilla, M. Sedighi, and J. P. Novak, "Performance enhancement of a multiresonant piezoelectric energy harvester for low frequency vibrations," *Energies*, vol. 12, no. 14, 2019, doi: 10.3390/en12142770.